

Optical conductivity of disordered graphene beyond the Dirac cone approximation

Shengjun Yuan¹, Rafael Roldán^{1,2}, Hans De Raedt³, and Mikhail I. Katsnelson¹

¹*Institute for Molecules and Materials, Radboud University of Nijmegen, NL-6525AJ Nijmegen, The Netherlands*

²*Instituto de Ciencia de Materiales de Madrid, CSIC, Cantoblanco E28049 Madrid, Spain*

³*Department of Applied Physics, Zernike Institute for Advanced Materials, University of Groningen, Nijenborgh 4, NL-9747AG Groningen, The Netherlands*

(Dated: October 29, 2018)

In this paper we systemically study the optical conductivity and density of states of disordered graphene beyond the Dirac cone approximation. The optical conductivity of graphene is computed by using the Kubo formula, within the framework of a full π -band tight-binding model. Different types of non-correlated and correlated disorders are considered, such as random or Gaussian potentials, random or Gaussian nearest-neighbor hopping parameters, randomly distributed vacancies or their clusters, and random adsorbed hydrogen atoms or their clusters. For a large enough concentration of resonant impurities, a new peak in the optical conductivity is found, associated to transitions between the midgap states and the Van Hove singularities of the main π -band. We further discuss the effect of doping on the spectrum, and find that small amounts of resonant impurities are enough to obtain a background contribution to the conductivity in the infra-red part of the spectrum, in agreement with recent experiments.

PACS numbers: 72.80.Vp, 73.22.Pr, 78.67.Wj

I. INTRODUCTION

An important part of our knowledge on the electronic properties of graphene, which consist of a two-dimensional (2D) lattice of carbon atoms,¹ can be deduced from optical spectroscopy measurements (for recent reviews see Refs. 2 and 3). Infrared spectroscopy experiments allows for the control of interband excitations by means of electrical gating,^{4,5} similarly as electrical transport in field effect transistors. Within the simplest Dirac cone approximation, only vertical in wave-vector space transitions across the Dirac point are optically active, leading to a constant value for the optical conductivity of undoped graphene of $\sigma_0 = \pi e^2/2h$. This leads to a frequency-independent absorption of $\pi\alpha \approx 2.3\%$, where $\alpha = e^2/\hbar c \approx 1/137$ is the fine structure constant. This fact was observed for suspended graphene in experiments in the visible range of the spectrum⁶ and it was later confirmed by further experiments in suspended graphene^{7,8} and epitaxial graphene on SiC substrate.⁹ For doped graphene with nonzero chemical potential μ , at zero temperature, in the absence of disorder and without considering many body effects, the allowed excitations are only those between particle-hole pairs with an energy difference larger than 2μ , due to Pauli's exclusion principle. This would lead to a zero infrared conductivity below the energy $\omega = 2\mu$, and the optical conductivity should be simply a step function $\sigma(\omega) = \sigma_0\Theta(\omega - 2\mu)$. However, a background contribution to the optical conductivity between $0 < \omega < 2\mu$ was observed in Refs. 5 and 7, pointing out the relevance of disorder and many body effects. Another characteristic of the optical spectrum is the Drude peak, which is built from a transfer of spectral weight from the low-energy interband conductance to the $\omega \rightarrow 0$ region of the spectrum,¹⁰ although

a strong suppression of the Drude peak at infrared energies has recently been observed.¹¹ Furthermore, the flattening of the π -bands at energies away from the Dirac point is responsible for the strong peak in the spectrum at higher energies (of the order of 5eV) which is associated to optical transitions between states of the Van Hove singularities.^{8,12,13} Finally, a method to control the intermediate excited states in inelastic light scattering experiments has been also reported, revealing the important role of quantum interference in Raman scattering.¹⁴

This intense experimental work has been accompanied by a series of theoretical studies which have treated the problem of the optical conductivity at different levels of approximation.¹⁵⁻²³ For example, it has been suggested that the presence of spectral weight in the *forbidden* region of the optical spectrum of doped graphene (below $\omega = 2\mu$) can be associated to disorder,^{15,24} electron-electron interaction²⁵ or excitonic effects.²⁶ In particular, the effect of electron interaction in the spectrum has been considered in Refs. 27-35. Furthermore, understanding the role played by the different kinds of disorder that can be present in this material is essential to increase the mobility of the samples. Besides the long-range charged impurities,^{22,36,37} other possible scattering sources such as ripples,³⁸ strong random on-site potentials,³⁹ large concentration of hydrogen adatoms,³⁹ strain^{40,41} or random deformations of the honeycomb lattice have been considered.^{42,43}

In this paper, we perform a systemic study of the optical spectrum of graphene with different kinds of disorder for both doped and undoped graphene, such as the randomness of the on-site potentials and fluctuation of the nearest-neighbor hopping. Special attention is paid to the presence of resonant impurities, e.g., vacancies and hydrogen adatoms, which have been proposed as the main factor limiting the carrier mobility in graphene.⁴⁴⁻⁴⁶

Furthermore, depending on the way how the defects are distributed over the lattice sites, each kind of disorder can be either non-correlated or correlated. The non-correlated one corresponds to the case with uniformly random distributed disorder sources, i.e., the potential or hopping are randomly changed within a certain range, or the resonant impurities (vacancies or hydrogen adatoms) are randomly positioned over the whole lattice; the correlated one means that the distribution of the disorder follow particular topological structures, such as Gaussian potentials or Gaussian hopping parameters, resonant clusters with groups of vacancies or hydrogen adatoms. In the present paper, we consider a noninteracting π -band tight-binding model on a honeycomb lattice and solve its time dependent Schrödinger equation (TDSE) to calculate the density of states (DOS). From this, the optical conductivity is calculated numerically by means of the Kubo formula.

The paper is organized as follows. In Sec. II we give details about the method. In Secs. III and IV we show results for the optical conductivity of undoped graphene in the presence of non-correlated and correlated disorder, respectively. In Sec. V we calculate the optical spectrum of doped graphene. Our main conclusions are summarized in Sec. VI.

II. MODEL AND METHOD

The tight-binding Hamiltonian of a disordered single-layer graphene is given by

$$H = - \sum_{\langle i,j \rangle} (t_{ij} a_i^\dagger b_j + \text{h.c.}) + \sum_i v_i c_i^\dagger c_i + H_{imp}, \quad (1)$$

where where a_i^\dagger (b_i) creates (annihilates) an electron on sublattice A (B), t_{ij} is the nearest neighbor hopping parameter, v_i is the on-site potential, and H_{imp} describes the hydrogen-like resonant impurities:

$$H_{imp} = \varepsilon_d \sum_i d_i^\dagger d_i + V \sum_i (d_i^\dagger c_i + \text{h.c.}), \quad (2)$$

where ε_d is the on-site potential on the “hydrogen” impurity (to be specific, we will use this terminology although it can be more complicated chemical species, such as various organic groups⁴⁴) and V is the hopping between carbon and hydrogen atoms. For discussions of the last term see, e.g. Refs. 39, 44, and 47. The spin degree of freedom contributes only through a degeneracy factor and is omitted for simplicity in Eq. (1). A vacancy can be regarded as an atom (lattice point) with and on-site energy $v_i \rightarrow \infty$ or with its hopping parameters to other sites being zero. In the numerical simulation, the simplest way to implement a vacancy is to remove the atom at the vacancy site.

The numerical calculations of the optical conductivity and DOS are performed based on the numerical solution

of the TDSE for the non-interacting particles. In general, the real part of the optical conductivity contains two parts, the Drude weight D ($\omega = 0$) and the regular part ($\omega \neq 0$). We omit the calculation of the Drude weight, and focus on the regular part. For non-interacting electrons, the regular part is^{39,48}

$$\sigma_{\alpha\beta}(\omega) = \lim_{\varepsilon \rightarrow 0^+} \frac{e^{-\beta\omega} - 1}{\omega\Omega} \int_0^\infty e^{-\varepsilon t} \sin \omega t \times 2\text{Im} \langle \varphi | f(H) J_\alpha(t) [1 - f(H)] J_\beta | \varphi \rangle dt, \quad (3)$$

(we put $\hbar = 1$) where $\beta = 1/k_B T$ is the inverse temperature, Ω is the sample area, $f(H) = 1/[e^{\beta(H-\mu)} + 1]$ is the Fermi-Dirac distribution operator, $J_\alpha(t) = e^{iHt} J_\alpha e^{-iHt}$ is the time-dependent current operator in the α ($= x$ or y) direction, and $|\varphi\rangle$ is a random superposition of all the basis states in the real space, i.e.,^{39,49}

$$|\varphi\rangle = \sum_i a_i c_i^\dagger |0\rangle, \quad (4)$$

where a_i are random complex numbers normalized as $\sum_i |a_i|^2 = 1$. The time evolution operator e^{-iHt} and the Fermi-Dirac distribution operator $f(H)$ can be obtained by the standard Chebyshev polynomial representation.³⁹

The density of states is calculated by the Fourier transform of the time-dependent correlation functions^{39,49}

$$\rho(\varepsilon) = \frac{1}{2\pi} \int_{-\infty}^\infty e^{i\varepsilon t} \langle \varphi | e^{-iHt} | \varphi \rangle dt, \quad (5)$$

with the same initial state $|\varphi\rangle$ defined in Eq. (4). For a more detailed description and discussion of our numerical method we refer to Ref. 39. In this paper, we fix the temperature to $T = 300\text{K}$. We use periodic boundary conditions in the calculations for both the optical conductivity and the density of states, and the size of the system is 8192×8192 or 4096×4096 .

III. NON-CORRELATED DISORDER

A. Random on-Site Potentials or Nearest-Neighbor Hopping Parameters

We first consider two different kinds of disorder: random local change of on-site potentials and random renormalization of the hopping, which correspond to the diagonal and off-diagonal disorders in the single-layer Hamiltonian Eq. (1), respectively. The former acts as a local shift of the chemical potential of the Dirac fermions, i.e., shifts locally the Dirac point, and the latter arises from the changes of distance or angles between the p_z orbitals. In order to introduce the non-correlated disorders in the on-site potentials, we consider that the on-site potential v_i is random and uniformly distributed (independently of each site i) between the values $-v_r$ and $+v_r$. Similarly,

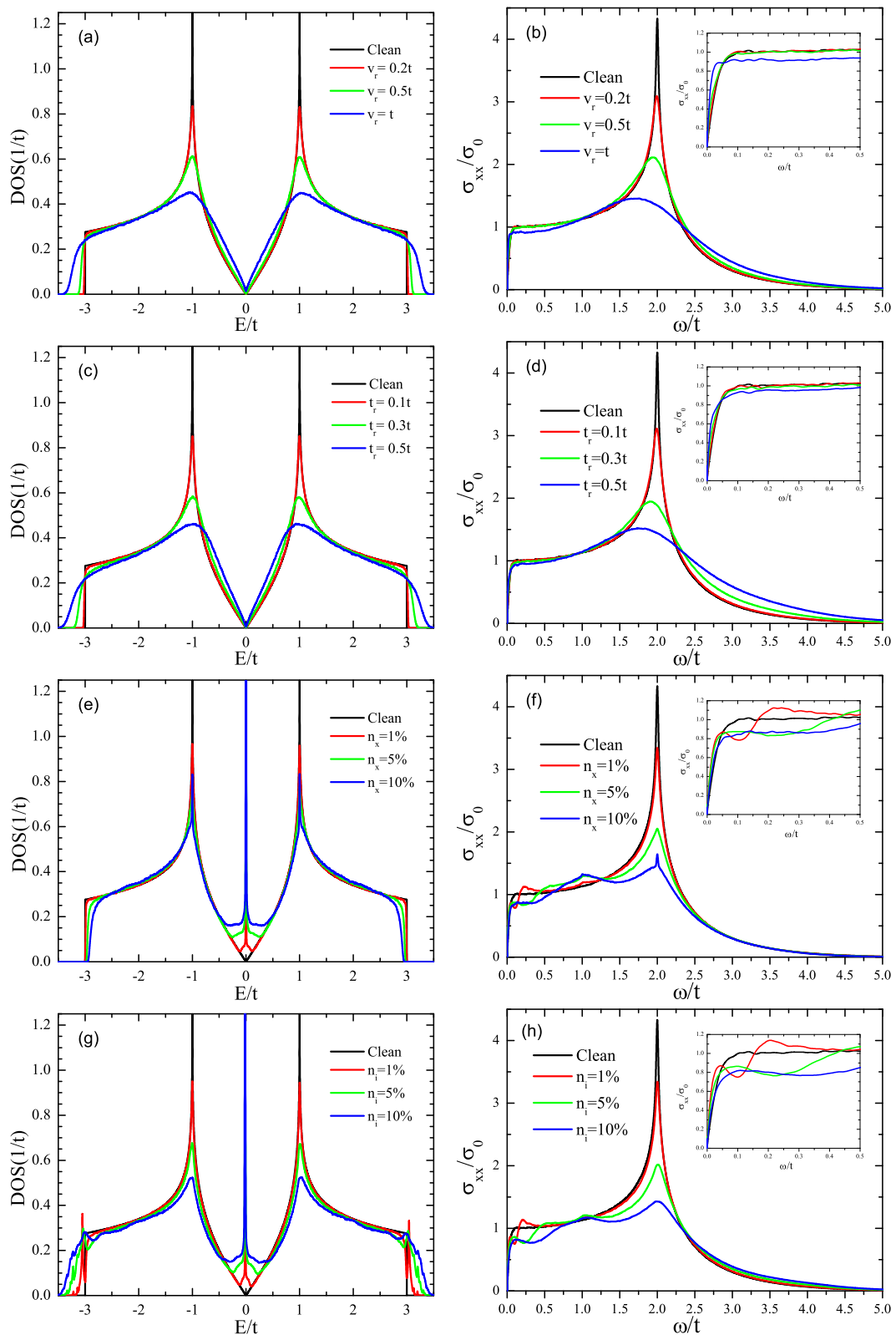


FIG. 1. (Color online) Numerical results for the density of states (left panels) and optical conductivity (right panels) of undoped graphene with different kinds of non-correlated disorders: (a,b) random on-site potentials, (c,d) random hopping parameters, (e,f) random distributed vacancies, and (g,h) random distributed hydrogen adatoms. Size of the samples is 4096×4096 for DOS, and 8192×8192 for optical conductivity. In the right column, the insets show a zoom of the optical conductivity in the infrared region of the spectrum.

the non-correlated disorder in the nearest-neighbor hopping is introduced by letting t_{ij} be random and uniformly distributed (independently of couple of neighboring sites $\langle i, j \rangle$) between $t - t_r$ and $t + t_r$. The presence of each type of disorder has quite similar effect to the density of states [see the numerical results with different magnitude of disorders in Fig. 1 (a) and (c) for the random on-site potentials ($v_r/t = 0.2, 0.5$ and 1) and random hoppings ($t_r/t = 0.1, 0.3$ and 0.5) respectively]. The spectrum is smeared starting from the Van Hove singularities at $|E| = t$, and the smeared region expands around their vicinal areas as the strength of the disorder is increased, whereas the spectrum around the vicinal region of the neutrality point keeps unaffected unless the disorder is too strong. As the optical conductivity is proportional to the density of states of the occupied and unoccupied states, one expects a peak in the spectrum of the optical conductivity at the energy $\omega \approx 2t$, which corresponds to particle-hole excitations between states of the valence band with energy $E \approx -t$ and states of the conduction band with energy $E \approx t$.⁵⁰ These processes contribute to the optical conductivity with a strong spectral weight due to the enhanced density of states at the Van Hove singularities of the π -bands. Because we are considering a full π -band tight-binding model for our calculations, this peak is also present in our results for the optical conductivity, as it is evident in Figs. 1(b) and (d) at $\omega/t \approx 2$, in qualitative agreement with recent experimental results.¹² Notice that the height of the peak is sensitive to the presence of disorder, getting more and more smeared as the strength of disorder is increased. On the other hand, for this kind of disorder, for which there is no big change in the DOS around the Dirac point, one expects that the low energy spectrum of the optical conductivity should be robust for small disorder, i.e., the optical conductivity should follow the same spectrum as the clean sample without any disorder. These expectations are exactly what we observed in the numerical results of $\sigma(\omega)$ shown in the insets of Fig. 1 (b) and (d). This is indeed the part of the spectrum that can be accounted for within the continuum (Dirac cone) approximation. We can conclude that the non-correlated random disorder in the on-site potentials or hopping integrals have almost no effect on the electronic properties (density of states and AC conductivity) in the low energy part of the spectrum unless the disorder is too large. On the other hand, the high energy inter-band processes between states belonging to the Van Hove singularities of the valence and conduction bands are quite sensitive to the strength of these two kinds of disorder.

B. Random Distributed Vacancies or Hydrogen Impurities

Next, we consider the influence of two other types of defects on graphene, namely, vacancies and hydrogen impurities. Introducing vacancies in a graphene sheet will

create a zero energy mode (midgap state), effect that has been anticipated in many theoretical works,^{17,39,51,52} and which has been recently observed experimentally by means of scanning tunneling spectroscopy (STM) measurements.⁵³ It is shown that the number of midgap states increases with the concentration of the vacancies³⁹, and the inclusion of vacancies brings an increase of spectral weight to the surrounding of the Dirac point ($E = 0$) and smears the van Hove singularities.^{17,39,52} This is in fact the behavior found in Fig. 1 (e) for the DOS of graphene with different concentrations of vacancies n_x , where the numerical results with $n_x = 1\%, 5\%, 10\%$ are represented and compared to the density of states of clean graphene.

The presence of hydrogen impurities, which are introduced by the formation of a chemical bond between a carbon atom from the graphene sheet and a carbon/oxygen/hydrogen atom from an adsorbed organic molecule (CH_3 , C_2H_5 , CH_2OH , as well as H and OH groups) have quite similar effect to the electronic structure and transport properties of graphene.^{39,44} The adsorbates are described by the Hamiltonian H_{imp} in Eq. (1). The band parameters $V \approx 2t$ and $\epsilon_d \approx -t/16$ are obtained from the *ab initio* density functional theory (DFT) calculations.⁴⁴ Following Refs. 39 and 44, we call these impurities as adsorbates hydrogen atoms but actually, the parameters for organic groups are almost the same.⁴⁴ As we can see from Fig. 1 (g), small concentrations of hydrogen impurities have similar effects as the same concentration of vacancies to the density of states of graphene. Hydrogen adatoms also lead to zero modes and the quasilocalization of the low-energy eigenstates, as well as to a smearing of the Van Hove singularities. The shift of the central peak of the density of states with respect to the Dirac point in the case of hydrogen impurities is due to the nonzero (negative) on-site potentials ϵ_d .

The similarity in the density of states leads to similar optical spectra for graphene with random vacancies or hydrogen adatoms, as it can be seen in Fig. 1 (f) and (h). In the high and intermediate energy part of the spectrum it is noticeable, apart from the smearing of the $\omega \approx 2t$ peak due to the renormalization of the Van Hove singularities, the appearance of a new peak at an energy $\omega \approx t$. This peak is associated to optical transitions between the newly formed midgap states (with energy $E \approx 0$) and the states of the Van Hove singularities (with energy $E \approx t$). Notice that, contrary to the $\omega \approx 2t$ peak, the height of this $\omega \approx t$ peak grows with the strength of disorder, due to the enhancement of the DOS at the Dirac point. Therefore, we expect that this peak should be observed in optical spectroscopy measurements of graphene samples with sufficient amount of resonant scatterers.

In the low energy part of the spectra, the new structure of the DOS around the Dirac point leads to a modulation of the infrared conductivity, as it can be seen in the insets of Figs. 1 (f) and (h). The lower peaks,

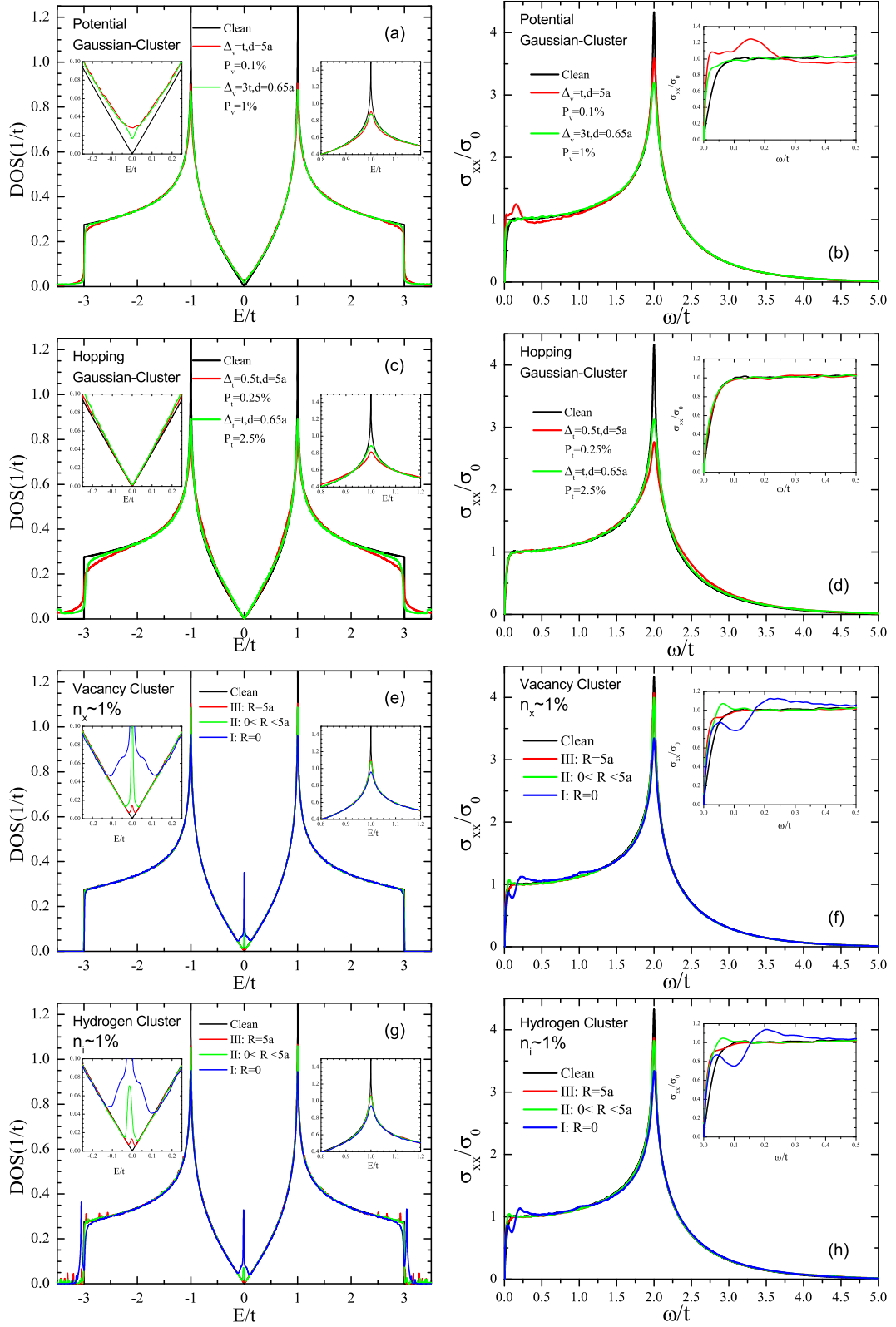


FIG. 2. (Color online) Numerical results for the DOS (left panels) and optical conductivity (right panels) of undoped graphene with different kinds of correlated disorders: (a,b) Gaussian potentials, (c,d) Gaussian hoppings, (e,f) vacancy clusters, and (g,h) hydrogen clusters. The distribution of the clusters of impurities used for the results (e)-(h) are sketched in Fig. 3.

which in Figs. 1 (f) and (h) corresponds to a conductivity $\sigma \approx 0.9\sigma_0$ for different concentration of impurities, might have their origin from excitations involving states surrounding the zero modes (central high peak in the density of states). At slightly higher energies there is a new set of peaks that can be associated to processes involving states at the boundaries of the midgap states. The optical conductivities in the region between these two peaks are in general smaller compared to those in clean graphene, which can be due to the fact that the midgap states are quasilocated states.

IV. CORRELATED DISORDERS

A. Gaussian Potentials and Gaussian Hoppings

As discussed in the previous section, the change of on-site potential can be regarded as a local chemical potential shift for the Dirac fermions. If the random potentials are too large, characteristics of the graphene band structure such as the Dirac points or the Van Hove singularities can disappear completely, and the whole spectrum becomes relatively flat over the whole energy range.⁵⁴ Therefore in order to introduce large values of random potentials but keep a relatively similar spectrum, in this section we use small concentrations of correlated Gaussian potentials, defined as^{54,55}

$$v_i = \sum_{k=1}^{N_{imp}^v} U_k \exp\left(-\frac{|\mathbf{r}_i - \mathbf{r}_k|^2}{2d^2}\right), \quad (6)$$

where N_{imp}^v is the number of the Gaussian centers, which are chosen to be randomly distributed over the carbon atoms (\mathbf{r}_k), U_k is uniformly random in the range $[-\Delta_v, \Delta_v]$ and d is interpreted as the effective potential radius. The typical values of d used in our model are $d = 0.65a$ and $5a$ for short- and long-range Gaussian potential, respectively. Here $a \approx 1.42\text{\AA}$ is the carbon-carbon distance in the single-layer graphene. The value of N_{imp}^v is characterized by the ratio $P_v = N_{imp}^v/N$, where N is the total number of carbon atoms of the sample. As one can see from Fig. 2(a), in the presence of locally strong disorders ($\Delta_v = 3t$ and t for short and long range Gaussian potentials, respectively) the whole spectrum of DOS is quite similar to the case of clean graphene, but with the emergence of states in the vicinal area around the Dirac point, and also a smearing of the Van Hove singularities. This kind of disorder leads to regions of the graphene membrane where the Dirac point is locally shifted to the electron ($U_k < 0$) or to the hole ($U_k > 0$) side with the same probability, rising the DOS at zero energy. The final spectrum is similar to the one of clean graphene but with a series of electron-hole puddles which are formed at the maxima and minima of the potential. The enhancement of the DOS around the Dirac point leads to the possibility for new excitations in the low energy part spectrum, as compared to the clean case, as it

can see in Fig. 2(b). For the cases we consider, the presence of long-range Gaussian potentials change the low energy optical spectrum completely with the emergence of a new peak around $\omega \approx 0.15t$. The optical conductivity in the region $\omega < 0.24t$ is larger than in clean graphene but becomes smaller for $\omega > 0.24t$. The increase of the conductivity might have its origin in the possible excitations between electron and hole puddles. Indeed, the renormalization of the spectrum obtained by considering long-range Gaussian potentials leads to a larger optical contribution than for short-range Gaussian potentials, which yield infra-red spectra much more close to that of a clean graphene membrane.

The local strong disorder in the hopping between carbon atoms is introduced in a similar way as the correlated potentials, i.e., with a distribution of the nearest-neighbor hopping parameter given by⁵⁴

$$t_{ij} = t + \sum_{k=1}^{N_{imp}^t} T_k \exp\left(-\frac{|\mathbf{r}_i + \mathbf{r}_j - 2\mathbf{r}_k|^2}{8d_t^2}\right), \quad (7)$$

where N_{imp}^t is the number of the Gaussian centers (\mathbf{r}_k), T_k is uniformly random in the range $[-\Delta_t, \Delta_t]$ and d_t is interpreted as the effective screening length. Similarly, the typical values of d_t are the same as for the Gaussian potential, i.e., $d_t = 0.65a$ and $5a$ for short- and long-range Gaussian random hopping, respectively, and the values of N_{imp}^t are characterized by the ratio $P_t = N_{imp}^t/N$.

Numerical results for the DOS and optical conductivity of graphene with short- ($\Delta_t = 3t$, $d_t = 0.65a$) and long-range ($\Delta_t = 1t$, $d_t = 5a$) Gaussian hoppings are shown in Fig. 2(c-d). This kind of disorder accounts for the effect of substitutional impurities like B or N instead of C, or local distortions of the membrane. Concerning the physics around the neutrality point, in this case the Dirac point remains unchanged although there is a local renormalization of the slope of the band. As a consequence, the Fermi velocity around Dirac is locally increased (when $t_k > 0$) or decreased (when $t_k < 0$). However, no midgap states are created by this kind of disorder, and the DOS remains quite similar to the one of a clean graphene layer, as it can be seen in Fig. 2(c). In particular, the absence of an impurity band at $E \approx 0$ makes that the optical conductivity presents only slight deviations as compared to the clean case. This can be seen in Fig. 2(d), where (apart from the smearing of the Van Hove peak) the optical spectrum, especially in the infra-red region, remains practically the same as in the absence of disorder.

B. Vacancy Clusters and Hydrogen Clusters

Correlated resonant impurities are introduced by the formation of groups of vacancies or adsorbed hydrogen atoms (see Fig. 3). The center of the formed vacancy

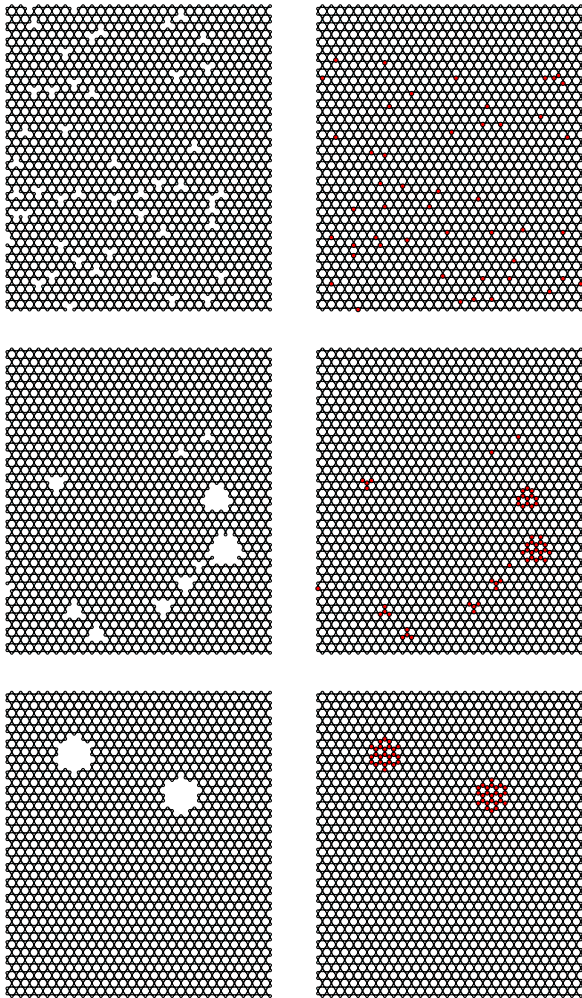


FIG. 3. (Color online) Sketch of a graphene sheet with vacancies (left panels) or hydrogen adatoms (right panels). The vacancies are presented as missing carbon atoms, whereas the hydrogen adatoms are highlighted in red. From top to bottom: Resonant impurities are distributed as the formation I ($R = 0$), II ($0 \leq R \leq 3a$) and III ($R = 3a$) as described in the text. For illustrative purposes, the size of the sample shown in this sketch is 60×40 , and the concentration of impurities is approximately equal to 2%.

or hydrogen cluster (\mathbf{r}_c) is randomly distributed over the honeycomb lattice sites, with equal probability on both sublattices A and B. Each site (i) whose distance to one of the centers ($R \equiv |\mathbf{r} - \mathbf{r}_c|$) is smaller than a certain value (R_c), is assumed to be part of the cluster, i.e., being a vacancy or adsorbing a hydrogen atom. We further introduce another freedom of the resonant clusters namely that their radius can change within the sample, allowing for a graphene layer with cluster of impurities of different size. This means that the value of R_c for each resonant cluster can either be different and randomly distributed to a maximum value, or can be kept fixed for all the clus-

ters in the sample. We want to emphasize that as the center of the cluster is located on a particular sublattice A or B, the formation of the cluster does not preserve the sublattice symmetry and therefore can lead to the appearance of midgap states.

First, in Fig. 2(e) and (g), we compare the density of states with the same total number of resonant impurities (vacancies or hydrogen adatoms) but with different kinds of formations. We consider three different situations, i.e., randomly distributed uncorrelated single impurities (formation I), randomly distributed correlated clusters with varied radius of clusters (formation II) or with fixed radius of clusters (formation III). The different structures are sketched in Fig. 3. Notice that the formation I is a limiting case of the formation III with all the radius of clusters being zero. As we can see from the results of the simulations, the number of midgap states is larger in the cases of uncorrelated single resonant impurities, and smaller for the case of fixed radius of resonant clusters. This is expected since the midgap states are states which are quasilocalized around the vacancies or carbon atoms which adsorb hydrogen atoms.^{17,39,51,52} Therefore, for the same concentration of impurities, the number of midgap states will grow with the *isolation* of the impurities in small clusters. Something similar happens for the case of hydrogen clusters. This can be understood by looking at Fig. 4, where we present contour plots of the amplitudes of quasieigenstates at the Dirac point or outside the midgap region. The quasieigenstate $|\Psi(\varepsilon)\rangle$ is a superposition of the degenerated eigenstates with the same eigenenergy ε , obtained by the Fourier transformation of the wave functions at different times³⁹

$$|\Psi(\varepsilon)\rangle = \frac{1}{2\pi} \int_{-\infty}^{\infty} dt e^{i\varepsilon t} |\varphi(t)\rangle, \quad (8)$$

where $|\varphi(t)\rangle = e^{-iHt} |\varphi\rangle$ is the time evolution of the initial state $|\varphi\rangle$ defined in Eq. (4). Although the quasieigenstate is not exactly the energy eigenstate unless the corresponding eigenstate is not degenerated at energy ε , we can still use the distribution of the amplitude in the real space to verify the quasilocalization of the zero modes in the presence of random impurities,³⁹ or obtain the DC conductivity at certain energies or carrier densities.^{39,44,54} As we can see from Fig. 4, the contour plots of the quasieigenstates of graphene with vacancy and hydrogen clusters are quite similar, i.e., the amplitudes on the carbon atoms which adsorb an hydrogen atom are almost zero, just like if they are vacancies. Furthermore, at the Dirac point (left panels of Fig. 4, corresponding to $E = 0$) the quasieigenstates are semi-localized around the edge of the clusters (see the red color in the regions around the cluster). On the other hand, for energies above the impurity band, the states are not localized around the resonant cluster, and the amplitudes of the quasieigenstates are more or less uniformly distributed over the sample except within the clusters, where the amplitudes are zero. Therefore, as we have discussed above, for a given concentration of im-

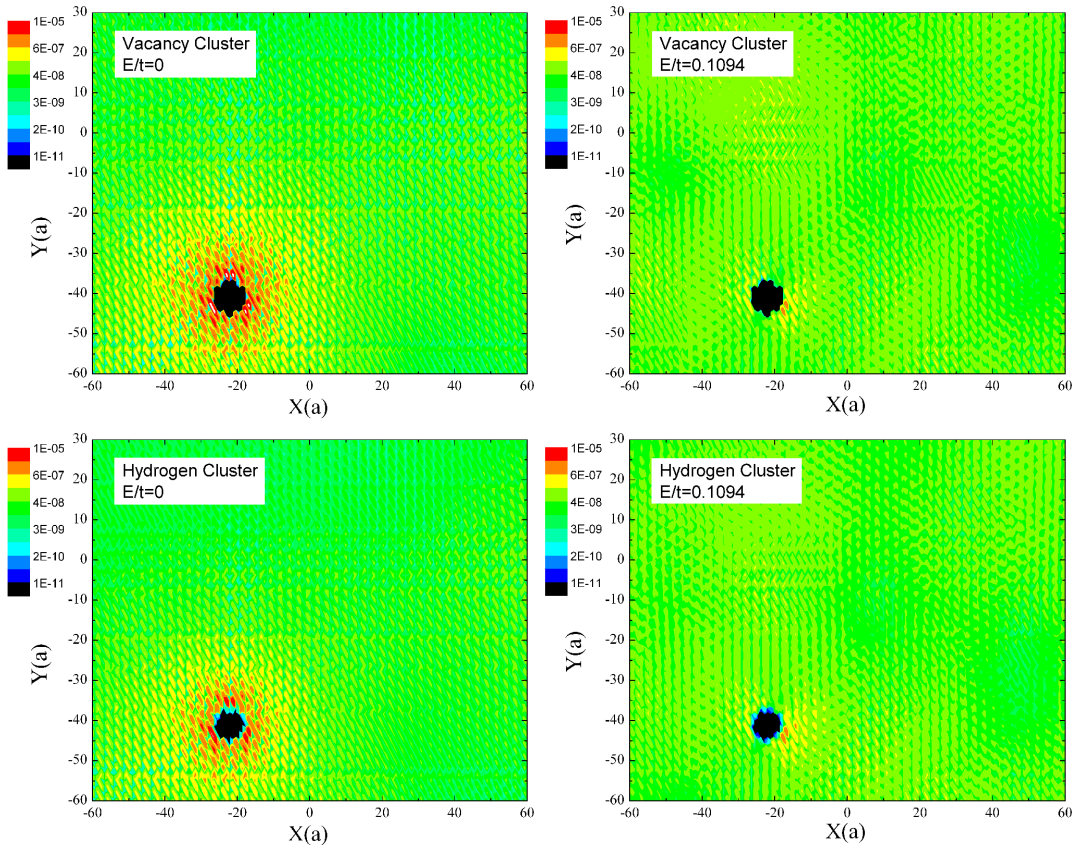


FIG. 4. (Color online) Contour plot of the amplitudes of quasideigenstates at energy $E = 0$ or $E = 0.1094t$. The radius of the resonant clusters is fixed at $R_c = 5a$.

purities, the number of carbon atoms which are located around an impurity will be larger in the formation I than in the formation III. Then, the number of zero modes is also larger in I than in III, leading to spectra for the DOS and optical conductivity similar to the ones of clean graphene for samples in which disorder is concentrated in a small number of big clusters (formation III) than spread into a large number of small clusters (formation I), as it can be seen in Figs. 2(e)-(h). Finally, notice that the possibility for new excitations between the impurity and the carrier bands, leads to a modulation of the optical conductivity (as compared to the clean membrane) whose peak structure depends on the renormalized DOS and band dispersion of each case.

V. OPTICAL CONDUCTIVITY OF DOPED GRAPHENE

So far we have discussed the effects of disorder on the optical response of undoped graphene. In this section, we study the optical conductivity of graphene for finite values of the chemical potential, taking into account the effect of disorder. At zero temperature, a clean sheet of gated (doped) graphene has a zero optical conductivity

in the region $\omega < 2\mu$, and an universal conductivity of $\sigma(\omega) = \sigma_0$, due to optically active inter-band excitations through the Dirac point, for energies above the threshold $\omega > 2\mu$.^{10,15,21,29,39} In the presence of the disorder, the broadening of the bands as well as the appearance of possible midgap states leads to a more complicated selection rule for the optical transitions, making possible to have excitations in the *forbidden region* $0 < \omega < 2\mu$, as observed experimentally.⁵ In this section, we are interested in studying the effect on the optical spectrum of doped graphene of the different kinds of disorder, considered in the previous section.

In Fig. 5 we compare the numerical results for the optical conductivity of doped graphene, considering four different types of non-correlated disorder (random potentials, random hoppings, vacancies and hydrogen adatoms) as well as clean graphene. First, one notice that the effect of doping is not relevant in the high energy part of the spectrum ($\omega \gg \mu$), and $\sigma(\omega)$ follows the same behavior discussed in Secs. III and IV, with a peak corresponding to particle-hole inter-band transitions between states of the Van Hove singularities at $\omega \approx 2t$. However, the spectrum changes dramatically in the infra-red region, as shown in the insets of Fig. 5. Therefore, from now on we will focus our interest on the effect of disorder

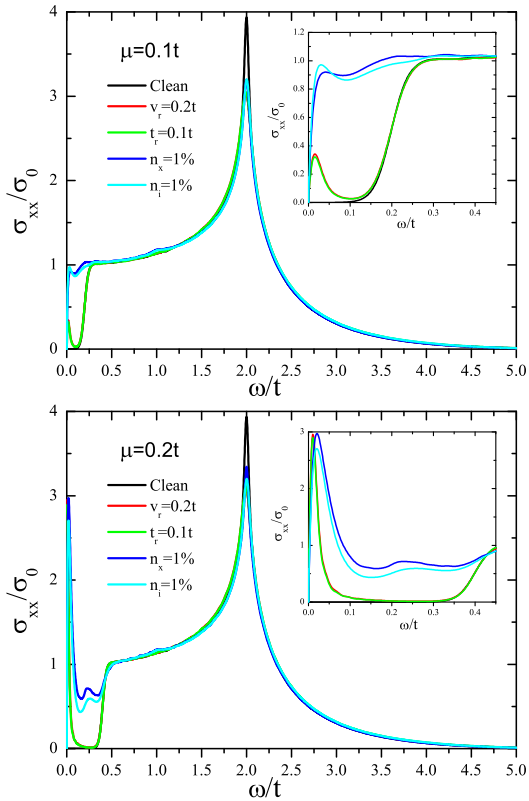


FIG. 5. (Color online) Simulation results of the optical conductivity of doped graphene with different kinds of non-correlated disorders. The chemical potential is $\mu = 0.1t$ in (a) and $0.2t$ in (b).

der on this low energy part of the spectrum. First, one notices that for all kinds of disorder, there is a peak in $\sigma(\omega)$ close to $\omega = 0$, whereas at slightly higher energies, $\sigma(\omega)$ drops to almost zero for the case of non-resonant scatterers (red and green curves), while there is still a non-zero background contribution when resonant scatterers are considered (light and dark blue curves). This can be understood as follows: for all the cases, disorder leads to a broadening of the bands, which allows for intra-band transitions between surrounding states of the Fermi level. However, we have seen that resonant impurities create an impurity band at the Dirac point, with the corresponding peak in the DOS at $E = 0$, whereas non-resonant impurities are not so effective in creating midgap states. Therefore, the background contribution that we find in Fig. 5(a)-(b) between $0 < \omega < 2\mu$ for samples with resonant scatterers are due to transitions between the newly formed impurity band and the conduction band. Taking into account that resonant impurities are believed to be the main source of scattering in graphene,^{44–46} our results suggest that this kind of impurities could be behind the background contribution to the optical conductivity observed experimentally.^{5,7,11,14} Finally, notice that the peak observed in $\sigma(\omega)$ for the case of resonant impurities at the energy $\omega \approx \mu$ is associ-

ated to transitions between the above discussed impurity band and states at the Fermi level.

To gain more insight about the effect of disorder in the optical conductivity of doped graphene, in Fig. 6 we show $\sigma(\omega)$ for different values of μ at fixed concentration of impurities (upper panels), and $\sigma(\omega)$ for different concentrations of impurities and fixed μ . In the first case, the main feature is that the conductivity increases as the doping decreases, in a qualitative agreement with the experimental results.⁵ When the chemical potential is fixed and the concentration of impurities changes (bottom panels), one observe that the conductivity in the region $0 < \omega < 2\mu$ grows with $n_{x(i)}$ from $\sigma(\omega) = 0$ for a clean sample to $\sigma(\omega) \approx 0.4\sigma_0$ for the larger concentration of impurities consider ($n_{x(i)} = 0.5\%$). If we compare to recent experiments, we notice that a 0.25% of resonant impurities would lead to a background contribution similar to the one reported by Li *et al.* for graphene on SiO₂,⁵ whereas only a $\sim 0.1\%$ of resonant impurities would be necessary to quantitatively reproduce the results of Chen *et al.* for graphene doped with a high-capacitance ion-gel gate dielectric.¹⁴ Finally, we can see that similar results are obtained when a sample with correlated on-site potential disorder distributed in the form of Gaussian clusters, as shown in Fig. 7. Therefore, we conclude that there are several kinds of disorder (resonant scatterers and correlated impurities) that can induce a finite conductivity in the infra-red region of the spectrum, as observed experimentally. It is the whole set of data on DC and AC transport from which one may infer the dominant type of defects in real graphene.

VI. CONCLUSION AND DISCUSSION

We have presented a detailed theoretical study of the optical conductivity of graphene with different kinds of disorder, as resonant impurities, random distribution of on-site potential or random renormalization of the nearest-neighbor hopping parameter (which can account for the effect of substitutional defects). Furthermore, we have consider the possibility for the impurities to be correlated or non-correlated.

For all types of disorder considered, the high energy peak at $\omega \approx 2t$, due to inter-band excitations between states of the Van Hove singularities of the valence and the conduction bands, are always sensitive to disorder, getting smeared out proportionally to the strength of disorder. On the other hand, the low energy part of the optical spectrum is strongly dependent on the type of disorder, as well as its strength and concentration. In general, for undoped graphene and in the presence of small disorder of the on-site potentials or in the nearest-neighbor hopping between the carbon atoms, the characteristics of the single-particle Dirac cone approximation are clearly present in the spectrum, and $\sigma(\omega) \approx \sigma_0$ at energies for which the continuum approximation applies. This is also true when we consider Gaussian hopping parameters. On

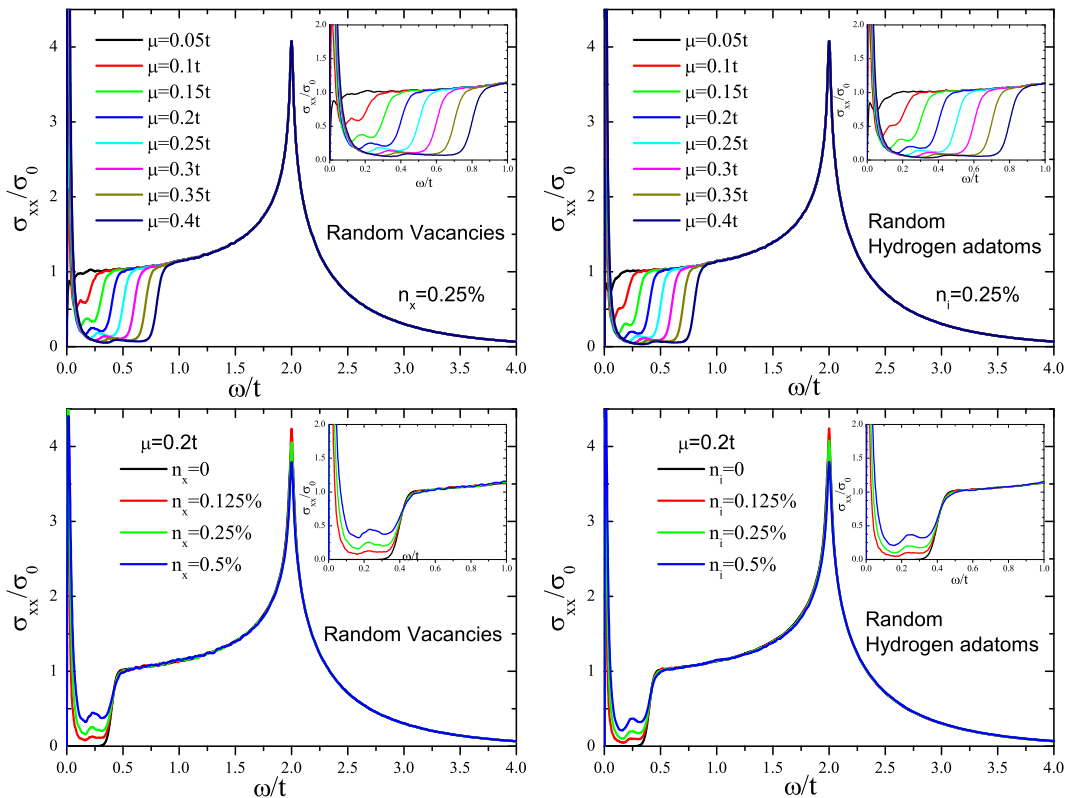


FIG. 6. (Color online) Optical conductivity of doped graphene with resonant scatterers. Upper panels: Fixed concentration of impurities, $\sigma(\omega)$ for different values of μ . Lower panels: Fixed chemical potential μ , $\sigma(\omega)$ for different concentration of impurities.

the other hand, if there are long-range Gaussian potentials, the local shifts of the Dirac points leads to electron-hole puddles and to the emergence of states in the vicinal region of the Dirac points. As a consequence, we observe an enhancement of the optical conductivity in the infra-red part of the spectrum. Interestingly, in the presence of resonant impurities (vacancies or hydrogen adatoms) there appear midgap states which are quasilo-calized around the impurities, the number of which is proportional to the number of carbon atoms which are located around the impurities. Completely random distributed (non-correlated) resonant impurities lead to the strongest enhancement of zero modes (seen as a prominent peak in the DOS at zero energy) and also the largest effect on the optical spectrum. In fact, for a large enough amount of resonant impurities, we obtain a new peak in the optical conductivity at an energy $\omega \approx t$, which is associated to optical transitions between the midgap states and states of the Van Hove singularities. When, for a given concentration of impurities, they merge together forming clusters, instead of staying uncorrelated, the influence of disorder on the electronic properties becomes smaller, especially if these clusters form large islands.

Finally, we have considered the effect of doping on the spectrum. Whereas for clean graphene, only inter-band processes with an energy larger than $\omega = 2\mu$ are optically active, the presence of disorder leads to a low energy peak in $\sigma(\omega)$ (associated to transitions near the Fermi level) plus a possible spectral weight in the region $0 < \omega < 2\mu$ for disorders that can create an impurity band at zero energy. Most importantly, we have found that a small amount of resonant impurities $\sim 0.1 - 0.2\%$, leads to a background contribution to $\sigma(\omega)$ between $0 < \omega < 2\mu$ in qualitative and quantitative agreement with recent spectroscopy measurements.

VII. ACKNOWLEDGEMENT

The authors thank useful discussions with E. Capelluti and F. Guinea. This research is supported by the Stichting Fundamenteel Onderzoek der Materie (FOM), the Netherlands National Computing Facilities foundation (NCF), the EU-India FP-7 collaboration under MONAMI and the grant CONSOLIDER CSD2007-00010.

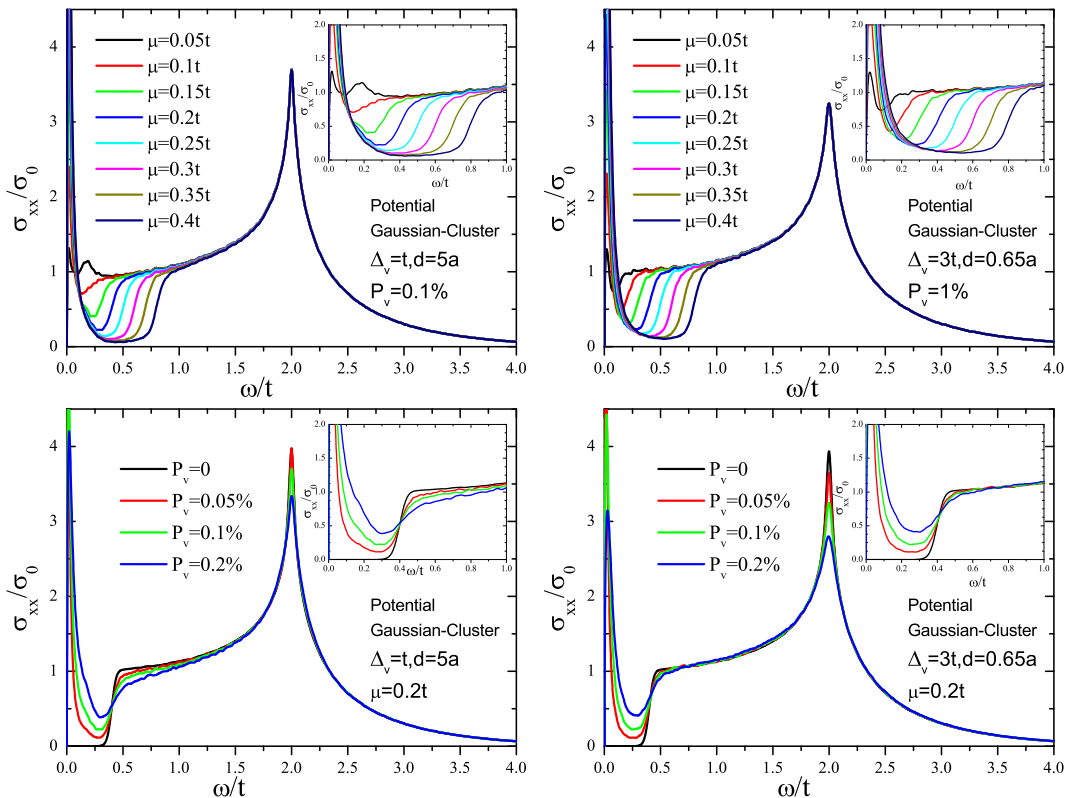


FIG. 7. (Color online) Same as Fig. 6 but for doped graphene with on-site potential disorder distributed in gaussian clusters.

- ¹ A. H. Castro-Neto, F. Guinea, N. M. R. Peres, K. Novoselov, and A. K. Geim, *Rev. Mod. Phys.* **81**, 109 (2009).
- ² N. M. R. Peres, *Rev. Mod. Phys.* **82**, 2673 (2010).
- ³ M. Orlita and M. Potemski, *Semicond. Sci. Technol.* **25**, 063001 (2010).
- ⁴ F. Wang, Y. Zhang, C. Tian, C. Girit, A. Zettl, M. Crommie, and Y. R. Shen, *Science* **320**, 206 (2008).
- ⁵ Z. Q. Li, E. A. Henriksen, Z. Jiang, Z. Hao, M. C. Martin, P. Kim, H. L. Stormer, and D. N. Basov, *Nature Physics* **4**, 532 (2008).
- ⁶ R. R. Nair, P. Blake, A. N. Grigorenko, K. S. Novoselov, T. J. Booth, T. Stauber, N. M. R. Peres, and A. K. Geim, *Science* **320**, 1308 (2008).
- ⁷ K. F. Mak, M. Y. Sfeir, Y. Wu, C. H. Lui, J. A. Misewich, and T. F. Heinz, *Phys. Rev. Lett.* **101**, 196405 (2008).
- ⁸ Z. Fei, Y. Shi, L. Pu, F. Gao, Y. Liu, L. Sheng, B. Wang, R. Zhang, and Y. Zheng, *Phys. Rev. B* **78**, 201402 (2008).
- ⁹ J. M. Dawlaty, S. Shivaraman, J. Strait, P. George, M. Chandrashekar, and F. Rana, *Phys. Rev. Lett.* **101**, 196405 (2008).
- ¹⁰ A. B. Kuzmenko, E. van Heumen, F. Carbone, and D. van der Marel, *Phys. Rev. Lett.* **100**, 117401 (2008).
- ¹¹ J. Horng, C.-F. Chen, B. Geng, C. Girit, Y. Zhang, Z. Hao, H. A. Bechtel, M. Martin, A. Zettl, M. F. Crommie, Y. R. Shen, and F. Wang, *Phys. Rev. B* **83**, 165113 (2011).
- ¹² K. F. Mak, J. Shan, and T. F. Heinz, *Phys. Rev. Lett.* **106**, 046401 (2011).
- ¹³ I. Santoso, P. K. Gogoi, H. B. Su, H. Huang, Y. Lu, D. Qi, W. Chen, M. A. Majidi, Y. P. Feng, A. T. S. Wee, K. P. Loh, T. Venkatesan, R. P. Saichu, A. Goos, A. Kotlov, M. Rübhausen, and A. Rusydi, *Phys. Rev. B* **84**, 081403 (2011).
- ¹⁴ C.-F. Chen, C.-H. Park, B. W. Boudouris, J. Horng, B. Geng, C. Girit, A. Zettl, M. F. Crommie, R. A. Segalman, S. G. Louie, and F. Wang, *Nature* **471**, 617 (2011).
- ¹⁵ T. Ando, Y. Zheng, and H. Suzuura, *Journal of the Physical Society of Japan* **71**, 1318 (2002).
- ¹⁶ A. Grüneis, R. Saito, G. G. Samsonidze, T. Kimura, M. A. Pimenta, A. Jorio, A. G. S. Filho, G. Dresselhaus, and M. S. Dresselhaus, *Phys. Rev. B* **67**, 165402 (2003).
- ¹⁷ N. M. R. Peres, F. Guinea, and A. H. Castro Neto, *Phys. Rev. B* **73**, 125411 (2006).
- ¹⁸ V. P. Gusynin, S. G. Sharapov, and J. P. Carbotte, *Phys. Rev. Lett.* **96**, 256802 (2006).
- ¹⁹ T. Stauber, N. M. R. Peres, and F. Guinea, *Phys. Rev. B* **76**, 205423 (2007).
- ²⁰ V. P. Gusynin, S. G. Sharapov, and J. P. Carbotte, *International Journal of Modern Physics B* **21**, 4611 (2007).
- ²¹ T. Stauber, N. M. R. Peres, and A. K. Geim, *Phys. Rev. B* **78**, 085432 (2008).
- ²² T. Stauber, N. M. R. Peres, and A. H. Castro Neto, *Phys. Rev. B* **78**, 085418 (2008).

- ²³ H. Min and A. H. MacDonald, Phys. Rev. Lett. **103**, 067402 (2009).
- ²⁴ N. M. R. Peres, T. Stauber, and A. H. C. Neto, EPL (Europhysics Letters) **84**, 38002 (2008).
- ²⁵ A. G. Grushin, B. Valenzuela, and M. A. H. Vozmediano, Phys. Rev. B **80**, 155417 (2009).
- ²⁶ N. M. R. Peres, R. M. Ribeiro, and A. H. Castro Neto, Phys. Rev. Lett. **105**, 055501 (2010).
- ²⁷ S. A. Mikhailov and K. Ziegler, Phys. Rev. Lett. **99**, 016803 (2007).
- ²⁸ E. G. Mishchenko, Phys. Rev. Lett. **98**, 216801 (2007).
- ²⁹ L. A. Falkovsky and S. S. Pershoguba, Phys. Rev. B **76**, 153410 (2007).
- ³⁰ L. A. Falkovsky and A. A. Varlamov, The European Physical Journal B - Condensed Matter and Complex Systems **56**, 281 (2007).
- ³¹ M. I. Katsnelson, EPL (Europhysics Letters) **84**, 37001 (2008).
- ³² R. Roldán, M. P. López-Sancho, and F. Guinea, Phys. Rev. B **77**, 115410 (2008).
- ³³ D. E. Sheehy and J. Schmalian, Phys. Rev. B **80**, 193411 (2009).
- ³⁴ V. Juričić, O. Vafek, and I. F. Herbut, Phys. Rev. B **82**, 235402 (2010).
- ³⁵ A. Giuliani, V. Mastropietro, and M. Porta, Phys. Rev. B **83**, 195401 (2011).
- ³⁶ T. Ando, Physica E: Low-dimensional Systems and Nanostructures **40**, 213 (2007), international Symposium on Nanometer-Scale Quantum Physics.
- ³⁷ F. de Juan, E. H. Hwang, and M. A. H. Vozmediano, Phys. Rev. B **82**, 245418 (2010).
- ³⁸ M. I. Katsnelson and A. K. Geim, Phil. Trans. R. Soc. A **366**, 195 (2008).
- ³⁹ S. Yuan, H. De Raedt, and M. I. Katsnelson, Phys. Rev. B **82**, 115448 (2010).
- ⁴⁰ V. M. Pereira, R. M. Ribeiro, N. M. R. Peres, and A. H. C. Neto, EPL (Europhysics Letters) **92**, 67001 (2010).
- ⁴¹ F. M. D. Pellegrino, G. G. N. Angilella, and R. Pucci, Phys. Rev. B **81**, 035411 (2010).
- ⁴² A. Cortijo and M. A. H. Vozmediano, Phys. Rev. B **79**, 184205 (2009).
- ⁴³ A. Sinner, A. Sedrakyan, and K. Ziegler, Phys. Rev. B **83**, 155115 (2011).
- ⁴⁴ T. O. Wehling, S. Yuan, A. I. Lichtenstein, A. K. Geim, and M. I. Katsnelson, Phys. Rev. Lett. **105**, 056802 (2010).
- ⁴⁵ M. Monteverde, C. Ojeda-Aristizabal, R. Weil, K. Ben-naceur, M. Ferrier, S. Guéron, C. Glattli, H. Bouchiat, J. N. Fuchs, and D. L. Maslov, Phys. Rev. Lett. **104**, 126801 (2010).
- ⁴⁶ Z. H. Ni, L. A. Ponomarenko, R. R. Nair, R. Yang, S. Anisimova, I. V. Grigorieva, F. Schedin, P. Blake, Z. X. Shen, E. H. Hill, K. S. Novoselov, and A. K. Geim, Nano Letters **10**, 3868 (2010).
- ⁴⁷ J. P. Robinson, H. Schomerus, L. Oroszlány, and V. I. Fal'ko, Phys. Rev. Lett. **101**, 196803 (2008).
- ⁴⁸ A. Ishihara, *Statistical Physics* (Academic Press, New York, 1971).
- ⁴⁹ A. Hams and H. De Raedt, Phys. Rev. E **62**, 4365 (2000).
- ⁵⁰ S. Yuan, R. Roldán, and M. I. Katsnelson, Phys. Rev. B **84**, 035439 (2011).
- ⁵¹ V. M. Pereira, F. Guinea, J. M. B. Lopes dos Santos, N. M. R. Peres, and A. H. Castro Neto, Phys. Rev. Lett. **96**, 036801 (2006).
- ⁵² V. M. Pereira, J. M. B. Lopes dos Santos, and A. H. Castro Neto, Phys. Rev. B **77**, 115109 (2008).
- ⁵³ M. M. Ugeda, I. Brihuega, F. Guinea, and J. M. Gómez-Rodríguez, Phys. Rev. Lett. **104**, 096804 (2010).
- ⁵⁴ S. Yuan, H. De Raedt, and M. I. Katsnelson, Phys. Rev. B **82**, 235409 (2010).
- ⁵⁵ C. H. Lewenkopf, E. R. Mucciolo, and A. H. Castro Neto, Phys. Rev. B **77**, 081410 (2008).